Acta Crystallographica Section B
Structural Science
ISSN 0108-7681

Aminoguanidinium(1+) pentafluorozirconate: multiple redetermination and comparisons

C. R. Ross II,[a] M. R. Bauer,[b]† R. M. Nielson[b]‡ and S. C. Abrahams[c]*

[a]Department of Structural Biology, St. Jude Children's Research Hospital, 332 North Lauderdale Street, Memphis, TN 38105-2794, USA, [b]Chemistry Department, Southern Oregon University, Ashland, OR 97520, USA, and [c]Physics Department, Southern Oregon University, Ashland, OR 97520, USA

† Present address: Department of Chemistry and Biochemistry, Arizona State University, Tempe, AZ 85287-1604, USA.
‡ Deceased 27 November 1998.

Correspondence e-mail: sca@mind.net

Received 19 February 2002
Accepted 15 July 2002

The structure of $CN_4H_7ZrF_5$ reported by Bukvetskii *et al.* [*Koord. Khim.* (1992). **18**, 576–579] has been independently redetermined on the basis of measurements on three different crystals. Assuming all four resulting structures are drawn from a normal distribution, normal probability analysis of the atomic coordinates taken in pairs reveals joint standard uncertainties that are underestimated by factors as large as 16.5 for the x(Zr) coordinate. Unit-cell parameters in the four crystals similarly have joint uncertainties, under the same assumption, that are underestimated by factors as large as 83.0 for the b axis. The variations in axial lengths from crystal to crystal and the declines in standard reflection intensities by 13–15% in at least two of the crystals measured are consistent with the inference that the distribution is not normal. Rather, the differences observed may be assumed to be caused by small but highly significant radiation-induced structural changes. The large underestimations hence reflect physical differences among the four irradiated crystals. The determinations show that the $CN_4H_7^{+1}$ cation is exactly planar except for the two H atoms bonded to the terminal N atom; the plane of this NH_2 group is normal to that of the cation. The average length of the three independent C—N bonds is 1.318 (11) Å; the N—N bond length is 1.397 (3) Å. Distorted ZrF_7 pentagonal bipyramids share edges, forming chains linked by N—H···F bonds to the $CN_4H_7^{+1}$ ions.

1. Introduction

The structural prediction that aminoguanidinium(2+) hexafluorozirconate, $(CN_4H_8)ZrF_6$, would exhibit ferroelectricity (Abrahams *et al.*, 1996) led to its preparation and the performance of the physical measurements required for investigation of this property (Bauer *et al.*, 2001). One preparation, using the method of Bukvetskii *et al.* (1990), yielded colorless transparent crystals of well developed morphology that differed markedly from the usual pale yellow products. A preliminary structure determination identified these crystals as aminoguanidinium(1+) pentafluorozirconate, $(CN_4H_7)ZrF_5$, the structure of which had been reported by Bukvetskii *et al.* (1992), hereafter B.

The latter reported y(F4) = 1/4, corresponding to Wyckoff position 4(c) rather than the actual 8(d) position, resulting in a composition $(CN_4H_7)ZrF_4$ instead of $(CN_4H_7)ZrF_5$. The Inorganic Crystal Structure Database (Bergerhoff *et al.*, 1983) later noted the given value of y(F4) was a printing error and replaced it by 0.532, without an estimate of uncertainty. Crystals (1) and (2) (see §2.2) were thereupon measured and the atomic coordinates redetermined. A comparison with B's corrected coordinates revealed maximum experimental deviates (see §3) of 4.7 for x(F1) in (1) and 23.0 for x(Zr) for (2).

© 2002 International Union of Crystallography
Printed in Great Britain – all rights reserved

Both terms have normal deviates of 2.36, hence either the coordinate differences are significant or the joint uncertainties are significantly underestimated. The combination of this result and the observed decay in standard reflection magnitudes of 13% in (1) and 15% in (2) led to the present investigation.

2. Experimental

2.1. Preparation and crystal growth

Aminoguanidinium(1+) pentafluorozirconate was initially prepared in a cation-exchange column by the reaction between $H_3O{\cdot}ZrF_5$ (acid fluorozirconate) and CN_4H_7Cl (aminoguanidinium chloride). The $H_3O{\cdot}ZrF_5$ was formed by the exchange of H_3O^+ with the K^+ ions in K_2ZrF_6. Subsequently, a more reproducible method proved to be the reaction between $CN_4H_6{\cdot}H_2CO_3$, $ZrF_4{\cdot}3H_2O$, HF and H_2O in a digestion bomb heated to 425 K (Bauer *et al.*, 1999). Evaporation of the resulting solution produced clear crystals once the concentration became greater than $\sim$0.12 g mL^{-1} in 0.28 *M* HF. Crystal (1) was prepared by the first method, (2) and (3) by the subsequent method.

2.2. Experimental data and refinement

A total of 1731 independent absorption-corrected reflections were measured on (1) at 295 (2) K with Mo $K\alpha$ radiation.[1] The standard reflection magnitudes declined 13% as a function of total exposure. Refinement gave $R_{int} = 0.030$, $R(F) = 0.028$ and $wR^2 = 0.076$.

For (2), 757 independent absorption-corrected reflections were measured at 200 (2) K using Cu $K\alpha$ radiation,[1] the standard reflection magnitudes declining 15% as a function of total exposure. Refinement gave $R_{int} = 0.036$, $R(F) = 0.019$ and $wR^2 = 0.046$.

The possibility that radiation-induced modification might have caused the substantial decline in standard intensities and a corresponding structural change, together with the uncertainty introduced by the use of empirical absorption corrections with the data from (1) and (2), led to new measurements on (3) (see Table 1). The long term (> 5 years) stability of $(CN_4H_7)ZrF_5$ crystals stored at room temperature in sealed but not evacuated vials contrasts strongly with the effects that occur rapidly under X-radiation for conditions that otherwise are identical. Many inorganic fluorides are known to be prone to chemical decomposition at elevated temperatures in the presence of water, hence (3) was placed in an Oxford Cryostream cryostat using dry N_2, then cooled to 283 (2) K. The lower temperature and drier conditions used reduced the maximum decline in the intensity standards to 1.85%.

[1] Supplementary data for (1) measured with Mo $K\alpha$ radiation, for (2) with Cu $K\alpha$ radiation and for (3) with Mo $K\alpha$ radiation are available from the IUCr electronic archives (Reference BR0112). Services for accessing these data are described at the back of the journal.

Table 1
Experimental details for (3).

Crystal data	
Chemical formula	$(CN_4H_7)ZrF_5$
M_r	261.308
Cell setting, space group	Orthorhombic, *Pnma* (62)
a, b, c (Å)	6.6485 (4), 6.9340 (4), 16.0344 (4)
V (Å^3)	739.20 (6)
Z	4
D_x (Mg m^{-3})	2.348
D_m (Mg m^{-3})	2.305 (5)
Radiation type	Mo $K\alpha$
No. of reflections for cell parameters	25
θ range (°)	20.056–23.888
μ (mm^{-1})	1.527
Crystal form	Polyhedral
Crystal size (mm)	0.27 × 0.105 × 0.090
$F(000)$	504
Data collection	
Diffractometer	Nonius MACH3
Data collection method	ω–2θ scans
Absorption correction	None
No. of measured, independent and observed reflections	3001, 1159, 1076
Criterion for observed reflections	$I > 2\sigma(I)$
R_{int}	0.0099
$2\theta_{min}$, $2\theta_{max}$ (°)	4.0, 60.0
Range of h, k, l	$-1 \rightarrow h \rightarrow 9$ $-1 \rightarrow k \rightarrow 9$ $-22 \rightarrow l \rightarrow 22$
No. and frequency of standard reflections	5 every 3600 s
Intensity decay	1.85%
Empirical intensity decay correction factors: min, max, mean	0.9997, 1.0117, 1.0029
Refinement	
Refinement on	F^2
$R[F > 4\sigma(F)]$, wR^2, S	0.0144, 0.0408, 1.199
No. of reflections and parameters used in refinement	All, 79
H-atom treatment	Mixed independent and constrained refinement
Weighting scheme	$w = 1/[\sigma^2(F_o^2) + (0.0087P)^2 + 0.1490P]$ where $P = (F_o^2 + 2F_c^2)/3$
$(\Delta/\sigma)_{max}$	−0.011
$\Delta\rho_{max}$, $\Delta\rho_{min}$ (e Å^{-3})	0.40, −0.29

Computer programs: *CAD*4 (Enraf–Nonius, 1989), *MaXus* (Mackay *et al.*, 1999), *SHELXL*97 (Sheldrick, 1997), *ORTEP* (Johnson, 1976).

2.3. Unit-cell dimensions and radiation-induced structural change

The unit-cell dimensions of $CN_4H_7ZrF_5$ measured on B, (1), (2) and (3) differ significantly (see Table 2). Apart from B, for which further information is unavailable, all remaining cell dimensions were measured at the termination of intensity data collection. The total exposure to radiation was 39, 60 and 60 h, respectively, for (1), (2) and (3). The unit-cell parameters averaged over all four sets are $a = 6.6454$, $b = 6.9134$, $c = 16.0176$ Å. The b axis in (1) and (3) exhibits the largest differences (Δ) between averaged and corresponding measured axial lengths, amounting to +83.0 and +51.5 Δ/σ, respectively, where σ is the estimated standard uncertainty derived by least-squares fit of the measured diffractometer angles to those in the model. If these differences were

Table 2
Unit-cell parameters for four $(CN_4H_7)ZrF_5$ crystals.

Crystal	a (Å)	b (Å)	c (Å)	λ (Å)	T_{meas}	$\Delta/\sigma(a)$	$\Delta/\sigma(b)$	$\Delta/\sigma(c)$
B†	6.640 (1)	6.875 (1)	15.999 (2)	Mo $K\alpha$	Not stated	−5.4	−38.4	−9.3
(1)†	6.6524 (5)	6.9466 (4)	16.0497 (9)	Mo $K\alpha$	295 (2)	+14.0	+83.0	+35.7
(2)‡	6.6404 (6)	6.8981 (5)	15.9872 (9)	Cu $K\alpha$	200 (2)	−8.3	−30.6	−33.8
(3)‡	6.6485 (4)	6.9340 (4)	16.0344 (4)	Mo $K\alpha$	283 (2)	+8.0	+51.5	+42.0
Average	6.6454	6.9134	16.0176					

† Prepared by the Bukvetskii *et al.* (1992) method. ‡ Prepared by the Bauer *et al.* (1999) method.

normally distributed, the joint uncertainties would be underestimated by factors of 56.7 and 35.2, respectively. The remaining (Δ/σ) ratios for all four crystals range from +42.0 to −38.4 for the b and c axes and between +14.0 and −8.3 for the a axis. These large ratios are unlikely to be due to random error in view of the systematic change in cell dimensions over the sequence B, (2), (3) and (1) (see Fig. 1). Together with the small but significant radiation-induced structural changes (RISC) detected in §3, the variation in Fig. 1 is more likely to be a function of the same changes. Each set of observed axial lengths could be fitted by the error function $y = A + B\,\mathrm{erf}[C(x-D)]$, shown as an aid for the eye by the curves in Fig. 1. It is noted (*a*) that a correlation, if any, between increasing RISC and the sense of the abscissa axis is presently undetermined, (*b*) that the equal spacing of crystal number entries along this axis is arbitrary, and (*c*) that the similarity of the three curves in Fig. 1 is strongly suggestive of a single RISC process.

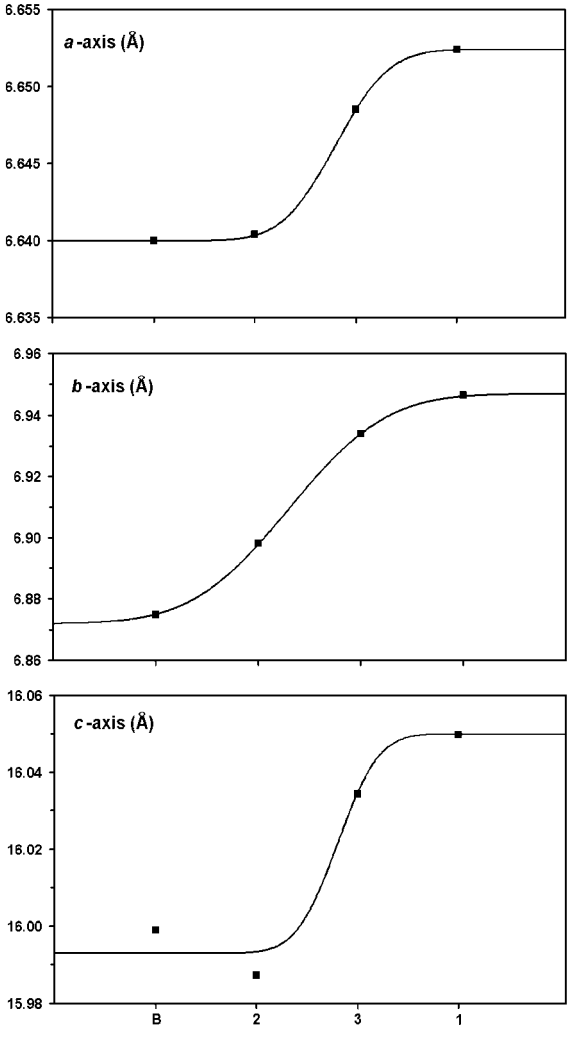

Figure 1
Variation of the *a*-axis, *b*-axis and *c*-axis lengths in B, (2), (3) and (1). The s.u. for each measurement is about the same size as the markers.

3. Normal probability analysis

3.1. Comparison of multiple independent structure determinations

Direct comparison of atomic coordinates and other parameters determined in independent structural investigations is readily made by normal probability analysis (Abrahams & Keve, 1971; Abrahams, 1997). The comparisons are made by calculating the experimental deviates $Q_{\mathrm{exp}(i)} = ([\xi_i(a) - \xi_i(b)]/\{\sigma^2[\xi_i(a)] + \sigma^2[\xi_i(b)]\})^{1/2}$, where $\xi_i(a)$ is the ith atomic coordinate magnitude in the ath study and $\xi_i(b)$ is the ith magnitude in the bth study. The expected modulus of $Q_{\mathrm{norm}(i)}$ for each ith normal deviate in a sample of size $n \geq i$ may be found in the *International Tables for X-ray Crystallography* (1974). If the plot of $Q_{\mathrm{exp}(i)}$ *versus* $Q_{\mathrm{norm}(i)}$ is linear, with unit slope and zero intercept, then the experimental deviates are consistent with a normal distribution and the ath and bth sets may be taken as free from systematic error unless both are subject to identical systematic error. A slope greater than unity indicates underestimation of the joint uncertainties, a smaller slope overestimation. Departure from linearity indicates uncorrected systematic error in the model.

A total of six pairwise normal probability analyses are possible on the basis of B's atomic coordinates and those derived from (1)–(3), as presented in Figs. 2(*a*)–2(*f*). Since no estimate of uncertainty in B's value of y(F4) was provided (see §1), its deviate is necessarily missing from the $Q_{\mathrm{exp}(i)}$ *versus* $Q_{\mathrm{norm}(i)}$ plots based on B's data. Each of Figs. 2(*a*)–2(*c*) hence contains 33 experimental deviates.

Determination of y(F4) and $\sigma[y(\mathrm{F4})]$ in the present refinements results in 34 experimental deviates in Figs. 2(*d*)–2(*f*). The largest resulting experimental deviate in all distributions, except for the case of Fig. 2(*a*), is that of x(Zr). $Q_{\mathrm{exp}}[x(\mathrm{Zr})]$ has magnitude 23.0 in Fig. 2(*b*), 7.1 in Fig. 2(*c*), 39.1 in Fig. 2(*d*), 11.9 in Fig. 2(*e*) and 34.1 in Fig. 2(*f*). The largest Q_{exp} in Fig. 2(*a*) is 4.7, for x(F1).

Each distribution contains additional $Q_{\rm exp}$ terms that depart significantly from a relatively linear array. The variable coordinate and $|Q_{\rm exp}|$ terms are z(N3) at 3.3 and z(F4) at 3.0 in Fig. 2(*a*); x(F3) at 5.2, x(N2) at 4.3, z(Zr) at 3.6 and z(F4) at 3.3 in Fig. 2(*b*); x(F1) at 4.2 and z(F4) at 3.9 in Fig. 2(*c*); z(Zr) at 8.9, x(F3) at 7.4 and z(F3) at 4.5 in Fig. 2(*d*); x(F4) at 5.1, z(Zr) at 3.6, x(F3) at 3.3 and z(C) at 2.0 in Fig. 2(*e*); and z(Zr) at 6.9, y(F4) at 6.8, x(F3) at 6.7, z(F3) at 4.9, x(F2) at 4.4 and x(N2) at 3.6 in Fig. 2(*f*).

Excluding all noted largest deviates, the fit to each remaining set of $Q_{{\rm exp}(i)}$ *versus* $Q_{{\rm norm}(i)}$ terms as determined by linear regression is shown by the straight lines in Figs. 2(*a*)–2(*f*). The resulting slopes are 1.23 (2), 1.74 (4), 1.32 (2), 1.64 (3), 1.19 (2) and 2.12 (3), respectively, each with an intercept in the range −0.1 to −0.3.

The largest experimental deviate has $|Q_{{\rm exp}(i)}| \geq 23$ in three separate distributions and is exclusively associated with (2) and the coordinate x(Zr). Crystal (2) is the only one with which Cu $K\alpha$ radiation was used and it exhibited the highest decline in standard intensities. The largest deviate magnitudes in two of the three other distributions, with $11.9 \geq Q_{{\rm exp}(i)} \geq 7.1$, are also associated with x(Zr). If the five terms that depart most from a normal distribution share a common origin, any structural change induced in (2) by radiation exposure is likely to be experienced similarly by both B and (1) (see §2.2).

The atomic coordinates from measurements on B and (1) agree more closely than those for any other pair of crystals [see Fig. 2(*a*)], with atomic coordinates for Zr that are strikingly similar. Mo $K\alpha$ radiation was used in both studies, with both crystals exposed to air at room temperature, hence both may be expected to undergo comparable radiation damage causing small but significant common atomic displacements.

The second and third largest experimental deviate in any distribution, with $8.9 \geq Q_{{\rm exp}(i)} \geq 7.4$, arises from the comparison of common atomic coordinates determined with (1) and (2) [see Fig. 2(*d*)]. As in the two other distributions involving (2), these large values of $Q_{\rm exp}$ are most likely associated with increased radiation-induced structural change in the crystal. The second, third and fourth largest experimental deviate in Fig. 2(*f*), with $6.9 \geq Q_{{\rm exp}(i)} \geq 6.7$, may again be associated with structural change produced in (2).

While the maximum observed difference of 0.0116 (7) Å in the location determined for x(Zr) is highly significant in terms of the refinement model and its associated uncertainties, with the maximum observed difference of 0.0025 (3) Å in z(Zr) also very significant, the crystal-chemical impli-

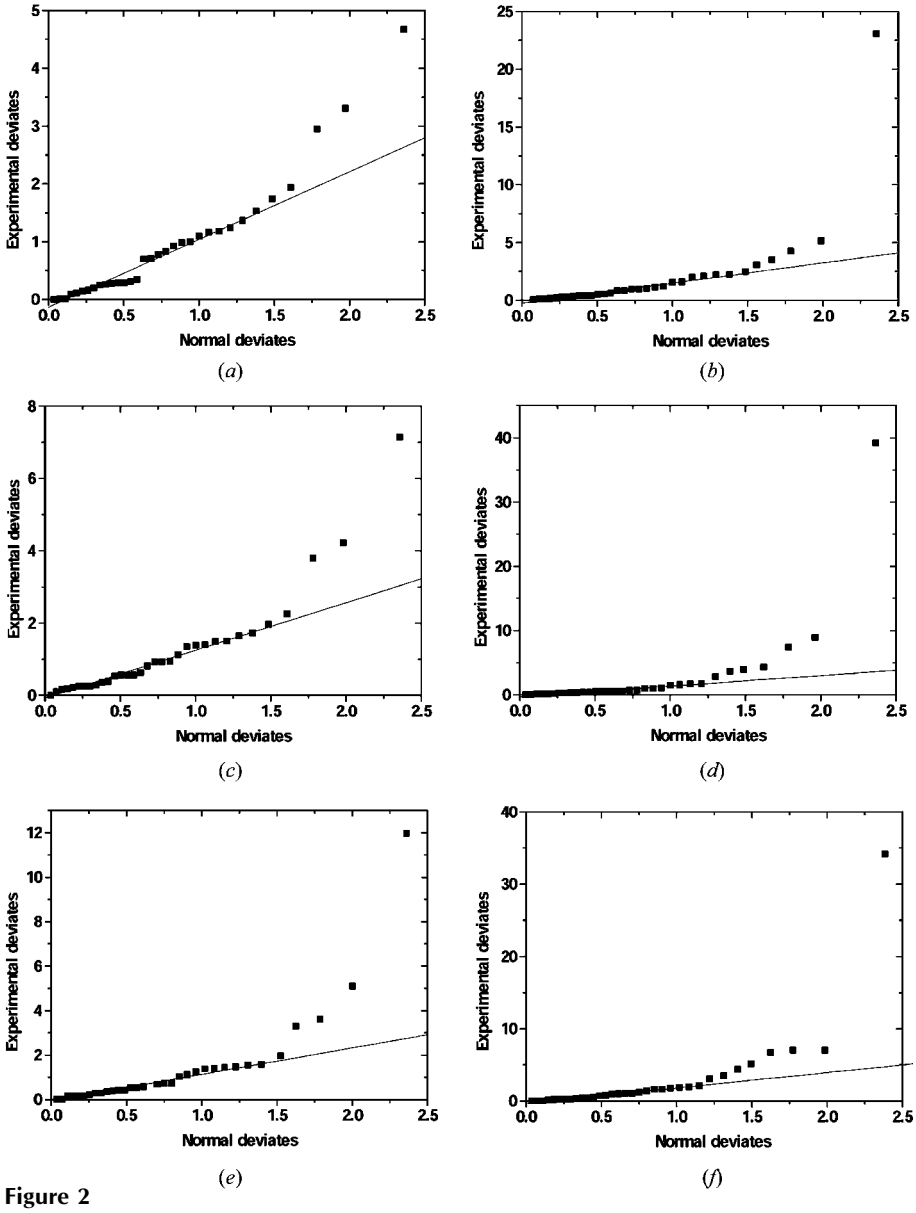

Figure 2
(*a*) Normal *versus* experimental deviates for the 33 atomic coordinates determined by Bukvetskii *et al.* (1992) and those in (1) (see §3.1). The line is given by linear regression, excluding the three largest experimental deviates. (*b*) Corresponding Q_i–Q_n plot for the 33 atomic coordinates determined by Bukvetskii *et al.* (1992) and those in (2). The line given by linear regression excludes the five largest experimental deviates. (*c*) Q_i–Q_n plot for the 33 atomic coordinates determined by Bukvetskii *et al.* (1992) and those in (3). The line given by linear regression excludes the three largest experimental deviates. (*d*) Q_i–Q_n plot for the 34 atomic coordinates determined in (1) and (2). The line given by linear regression excludes the four largest experimental deviates. (*e*) Q_i–Q_n plot for the 34 atomic coordinates determined in (1) and (3). The line given by linear regression excludes the five largest experimental deviates. (*f*) Q_i–Q_n plot for the 34 atomic coordinates determined in (2) and (3). The line given by linear regression excludes the seven largest experimental deviates.

cations involve minor shifts only in the minima locations.

All linear regression slopes in the distributions shown in Figs. 2(*a*)–2(*f*) exceed unity and are indicative of joint standard uncertainties in these normally distributed experimental deviates that are too small by factors corresponding to each slope, ranging from 1.19 (2) to 2.12 (3). Least-squares underestimation of the uncertainty in refined atomic coordinates, by factors that range from $2^{1/2}$ to 2, is common (Hamilton & Abrahams, 1970). Such a range is closely comparable to that in the present distributions if outliers are excluded, but the highly significant underestimation in calculated uncertainties associated with the heaviest atom present does not appear to have been reported previously. The value $Q_{\rm exp}[x({\rm Zr})] = 39.1$ in Fig. 2(*d*) has a normal deviate value 2.37, hence $\sigma[x({\rm Zr})]$ is underestimated by the factor 16.5; in Figs. 2(*b*), 2(*c*), 2(*e*) and 2(*f*), the corresponding underestimation factor is 9.7, 3.0, 5.0 and 10.4, respectively. Structural determination based on the investigation of one single crystal does not detect systematic underestimation, hence the present finding may be widely applicable in the presence of RISC, as indicated by significant declines in standard reflection intensity magnitudes.

3.2. Lattice constants and radiation-induced structural change

The unit-cell dimensions of a stable phase in a material of given composition and order at a standard temperature and pressure are highly reproducible. Variations in these dimensions, other than those due to random experimental error, are generally caused by a departure in one or more variables from standard. The unexpectedly large and systematic departures from average of individual unit-cell dimensions in §2.3 exceed those due to temperature or pressure changes. The departures can, however, be correlated with changes such as the maximum observed difference of 0.0116 (7) Å in x(Zr) for (1) and (3), a distance close to the maximum observed difference in *a*-axis length. The combined observation of systematically variable unit-cell parameters, variable atomic coordinates and a significant decline in the intensity of standard reflections is fully compatible with small but significant structural change induced by radiation exposure.

It is notable that the interatomic distances in (1) and (2) do not differ significantly from those in (3).

3.3. Heavy-atom-containing materials subject to radiation-induced change

The possibility has been raised in this study that least-squares-derived uncertainties in the atomic coordinates of the heaviest atom(s) present, in addition to those of one or more lighter atoms, may be unexpectedly underestimated in the event that the crystal studied is susceptible to structural change caused by radiation exposure. A decline in the intensity standards greater than $\simeq$5% may be the first indicator of such susceptibility.

A test for this possibility is the determination of lattice constants in three or more different crystals of the candidate material, each of which has been exposed differently to X-radiation. Greater variation than expected in a normal distribution may indicate RISC. In the event of a variation larger than normal, structural determination on three or more crystals followed by pairwise comparison of the resulting atomic coordinates in $Q_{{\rm exp}(i)}$–$Q_{{\rm norm}(i)}$ plots provides definitive confirmation. Structural determinations based on the investigation of multiple crystals are expected to reveal the extent to which RISC and the associated but otherwise undetected and unexpected increase in the uncertainty of the refined atomic coordinates is common.

Table 3
Selected interatomic distances (Å) and angles (°) in $(CN_4H_7)ZrF_5$ for (3).

Zr—F3	1.959 (1)	C—N4	1.310 (3)
Zr—F4^{i}	1.963 (1) ×2	C—N3	1.313 (3)
Zr—F1	2.096 (1)	C—N1	1.330 (3)
Zr—F2^{ii}	2.137 (1)		
Zr—F1^{ii}	2.154 (1)	N1—N2	1.397 (3)
Zr—F2	2.183 (1)		
		N3—C—N4	121.7 (2)
N3—H3	0.83 (3)	N1—C—N4	119.3 (2)
N3—H4	0.87 (3)	N1—C—N3	119.0 (2)
N4—H5	0.91 (3)	C—N1—N2^{iii}	119.4 (2)
N4—H6	0.76 (3)		
N1—H1	0.84 (4)	H4—H5	2.41 (4)
N2—H2	0.83 (2)	H3—H4	1.40 (4)
		H3—H1	2.30 (5)
H5—H6	1.48 (4)	H6—N2^{iii}	2.28 (3)
H2—H2′	1.27 (4)		

Symmetry codes: (i) $x, \frac{1}{2}-y, z$; (ii) $x-\frac{1}{2}, y, \frac{1}{2}-z$; (iii) $x-\frac{1}{2}, y, \frac{3}{2}-z$.

4. Structural results and discussion

4.1. Aminoguanidinium(1+) and (2+) ion geometry

The bond lengths and angles derived from the atomic coordinates (see supplementary material), many of which differ significantly from those of B, are presented in Table 3; a view of the $(CN_4H_7)^{1+}$ ion is shown in Fig. 3(*a*). The calculated standard uncertainties in Table 3 are smaller than B's by a factor of $\sim$2. Ten of the 12 atoms in the $(CN_4H_7)^{1+}$ ion are located on the mirror plane at $y = 1/4$ and are hence exactly coplanar; the line joining the remaining atoms H2′ and symmetry related H2″ [see Fig. 3(*a*)] is normal to the molecular plane. The bond angles about the planar C atom are slightly distorted, with N3—C—N4 significantly larger, and N1—C—N3 and N1—C—N4 barely significantly smaller, than 120°. The distortion may be associated with the C—N1 bond, which is significantly longer than the C—N3 and C—N4 bonds. Analysis of 177 reports on the dimensions of the $(H_2N)_2$—C—N$<^{\rm H}$ fragment in the Cambridge Structural Database (Allen & Kennard, 1993) reveals a mean $d_{\rm C-N} = 1.323$ (1) Å for the equivalent of the present C—N3 and C—N4 bonds and a mean $d_{\rm C-N} = 1.335$ (2) Å for the equivalent of the C—N1 bond. The latter mean is in good agreement with the results in Table 3, but the C—N3 and C—N4 bond lengths in the table are significantly shorter than the mean values from the database. This may be due to interactions with the hydrogen bonds, which amount to 0.10–0.15 valence units (v.u.) for each of the four H atoms involved

Table 4
Selected N—H···N,F hydrogen bonds, with length in Å, angle in ° and bond valence in valence units for (3).

N—H	$d_{H\cdots N,F}$	N—H···N,F	$d_{N\cdots N,F}$	N,F	v.u.†
N3—H4	2.01 (3)	177 (3)	2.879 (3)	F3	0.103 (6)
N4—H5	2.12 (3)	180 (3)	3.031 (2)	F2	0.083 (4)
N4—H6	2.28 (3)	112 (3)	2.659 (3)	N2	0.108 (6)
N4—H5	2.35 (3)	112 (2)	2.817 (2)	F1	0.058 (2)
N3—H3‡	2.43 (3)	139 (1)	3.103 (2)	F4	0.052 (2)
N2—H2	2.43 (3)	146 (2)	3.154 (2)	F4	0.052 (2)
N1—H1‡	2.49 (3)	118 (2)	2.980 (2)	F4	0.047 (2)
N4—H6	2.51 (3)	149 (3)	3.189 (3)	F3	0.046 (2)

† Brown & Altermatt (1985). ‡ Bond bifurcated by symmetry.

(Brown & Altermatt, 1985) (see Table 4). The shortest N—H···F bond formed has $d_{H\cdots F} = 2.01$ Å, with N3—H4···F3 = 177.1°; others are given in Table 4.

In the present study, $\langle d_{C-N}\rangle = 1.318\ (11)$ Å is in close agreement with $d_{C-N} = 1.322\ (8)$ Å in the $(CN_4H_7)^{1+}$ ion of $(CN_4H_7)_2SiF_6{\cdot}2H_2O$ (Ross *et al.*, 1999), 1.323 (21) Å in the $CN_4H_8^{2+}$ ion of $CN_4H_8ZrF_6{\cdot}H_2O$ (Ross *et al.*, 1998) and 1.320 (8) Å in $(CN_4H_7)^{1+}NO_3^-$ (Akella & Keszler, 1994). A total of 795 observations for the guanidinium moiety $[(NH_2)_2CNX]$ in the Cambridge Structural Database yields $\langle d_{C-N}\rangle = 1.32\ (2)$ Å, with no significant difference between the H_2N-C bonds and the $C-NX$ bond nor among the three N—C—N bond angles. The comparable heterocyclic C—N bond length in the planar C_4N_2 ring of thiamin acetate (Casas *et al.*, 1994) is 1.339 (3) Å.

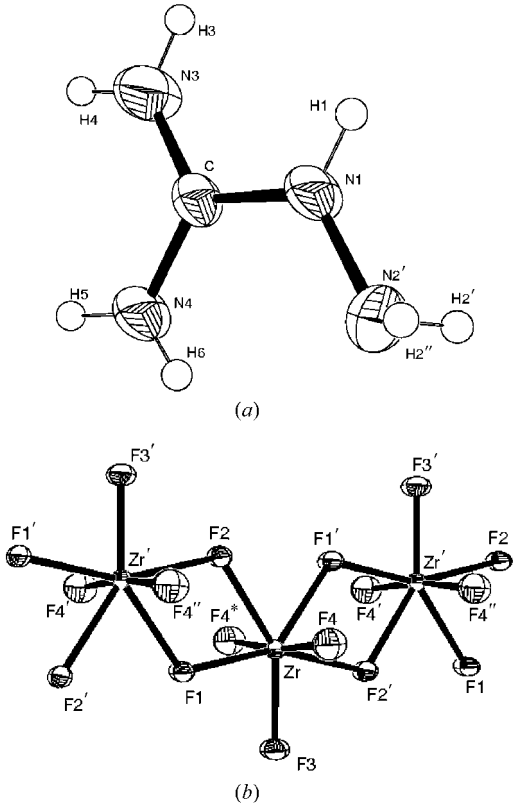

Figure 3
(*a*) Aminoguanidinium(1+) ion in aminoguanidinium(1+) pentafluorozirconate. (*b*) Three edge-sharing ZrF_7^{-4} ions in aminoguanidinium(1+) pentafluorozirconate. Symmetry code (′) $\frac{1}{2}+x, \frac{1}{2}-y, \frac{1}{2}-z$; (″) $\frac{1}{2}+x, y, \frac{1}{2}-z$; (*) $x, \frac{1}{2}-y, z$.

4.2. Fluorozirconate ion geometry

The unit cell of $(CN_4H_7)ZrF_5$ contains Zr atoms in seven-coordination rather than isolated ZrF_5^- ions, with average $\langle d_{Zr-F}\rangle = 2.07\ (10)$ Å (see Table 3). Distorted bipyramids share common F1–F2 edges between adjacent pairs of polyhedra, the infinite chains thereby formed maintaining stoichiometry [see Figs. 3(*b*) and 4]. Shannon (1976) gives $d_{Zr-F} = 2.08$ Å, assuming an average coordination of three for F^-, which is in close agreement with the present value. The calculated Zr—F bond strengths (Brown & Altermatt, 1985) in the pentagonal bipyramidal polyhedra are Zr—F1 = 0.505 v.u., Zr—F1′ = 0.435 v.u., Zr—F2 = 0.402 v.u., Zr—F2′ = 0.456 v.u., Zr—F3 = 0.737 v.u. and Zr—F4 (×2) = 0.728 v.u. for a total valence of 3.994, in excellent agreement with expectation for Zr^{4+}. Atoms F3 and F4 form bonds with only one Zr atom and are shorter than ∼2.0 Å; by contrast, F1 and F2 are shared by two Zr atoms and are longer than ∼2.0 Å (see Table 3). Similar differences between shared and unshared Zr—F bonds are noted in other fluorozirconates. The $Zr_4F_{24}^{8-}$ anion in the monohydrate $CN_4H_8ZrF_6{\cdot}H_2O$ contains both shared and unshared Zr—F bonds, the shared bond with $\langle d_{Zr-F}\rangle = 2.18\ (3)$ Å, the unshared with $\langle d_{Zr-F}\rangle = 2.05\ (3)$ Å (Ross *et al.*, 1998). In α-ZrF_4, however, no significant difference is reported between shared and unshared $\langle d_{Zr-F}\rangle$ bond lengths, which range from 2.031 (2) to 2.190 (2) Å (Papiernik *et al.*, 1982).

4.3. Relative stability of pentafluorozirconate and hexafluorozirconate ions

The geometry of Zr(IV)-halide complexes varies with halide:Zr ratio, the d^0 Zr(IV) ion exerting no geometrical

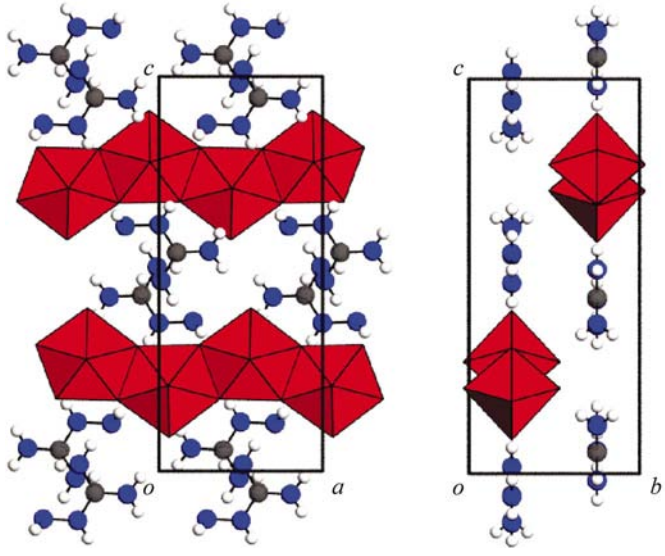

Figure 4
Packing of $(CN_4H_7)^{+1}$ and ZrF_7^{-4} ions in unit cell.

bonding preference, with several aminoguanidinium fluorozirconates reported (Davidovich *et al.*, 1982). The compositional dependence of both ions on pH is also a source of variation. Aminoguanidine can form $CN_4H_7(1+)$ or $CN_4H_8(2+)$ ions by two-step protonation in acidic media: (*a*) $CN_4H_6 + H^+ \Leftrightarrow CN_4H_7^+$ and (*b*) $CN_4H_7^+ + H^+ \Leftrightarrow CN_4H_8^{2+}$. Solutions of fluorozirconate ions similarly undergo equilibria (*c*) $ZrF_6^{2-} + H^+ \Leftrightarrow ZrF_5^- + HF$ and (*d*) $ZrF_5^- + H^+ \Leftrightarrow ZrF_4 + HF$. Nolan (1967) showed that the equilibrium $ZrF_{n-1} + HF \Leftrightarrow ZrF_n + H^+$ favors the formation of ZrF_6^{2-} for HF concentration greater than 1 *M*. Below this concentration, the composition ZrF_5^- forms. Solutions with high HF concentration hence yield $CN_4H_8ZrF_6$, those with lower concentration $(CN_4H_7)_2ZrF_6$ and those at still lower HF concentration $CN_4H_7ZrF_5$ (Bauer *et al.*, 1999).

Calorimetric measurement (unpublished) shows that $CN_4H_8ZrF_6$ loses HF rapidly above 450 K, more slowly at lower temperatures. The following decomposition scheme is found: (*a*) $CN_4H_8ZrF_6 \Rightarrow CN_4H_7ZrF_5 + HF$, then (*b*) $CN_4H_7ZrF_5 \Rightarrow CN_4H_6 + ZrF_4 + HF$. At higher temperatures, ZrF_4 may oxidize to ZrO_2, as reported in the thermal decomposition of $(NH_4)_2ZrF_6$ by Rodriguez *et al.* (1985).

4.4. Atomic displacement parameters in $CN_4H_7ZrF_5$

The crystal structure of $CN_4H_7ZrF_5$ (see Fig. 4) has been basically described by Bukvetskii *et al.* (1990). The atomic displacement parameters (a.d.p.s) in (3) for Zr, F, N and C have $U^{22} > U^{11}$, U^{33} except for F4, the displacements hence being largest normal to the cation plane [see Figs. 3(*b*) and 4]. The possibility that the thermal-ellipsoid elongation might result from the lack of an absorption correction was investigated by applying a correction based on ψ scans and then repeating the refinement. The results suggest a weak correlation between the elongation and the absorption correction,[2] with R_{int} increasing slightly to 0.0108, R to 0.0163 and wR^2 to 0.0472 (see Table 1 for previous values). The refinement is hence reported without absorption correction.

The observed relation among the a.d.p.s may be caused by several effects, including (*a*) the truncation of data along the b^* direction, (*b*) at least partially anisotropic RISC and (*c*) the presence of unsuspected positional disorder. However, not only is there no indication in the data of (*a*) or (*b*), but both are expected to affect all atoms approximately equally, whereas the thermal ellipsoid of F4 has a maximum value near the U^{11} direction. If it is assumed that the a.d.p.s correspond to libration about the chain axis, then it would be expected that $U^{22}(F1) \simeq U^{22}(F2) < U^{22}(F3)$, whereas $U^{22}(F2) < U^{22}(F1) < U^{22}(F3)$ with nearly equal differences of $\sim 8\sigma$, and that $U^{33}(F4)$ would be the largest displacement for that atom, whereas it is the smallest. It is noted that F1 is about 0.2% overbonded to Zr, F2 about 6.0% underbonded.

[2] The largest positional changes resulting from refinement, following application of the absorption correction, were about two standard uncertainties (s.u.) in z(H3) and y(H2). No change in U^{11} exceeded 1 s.u., but all U^{22} changes were negative, with the largest −7.3 s.u. for Zr and two others (F1 and F4) less than 2 s.u. The largest change in U^{33} was −3.9 s.u. for Zr, with all others less than about 1 s.u. and no change in $U^{13} > 1$ s.u.

Although ellipsoidal elongation is consistent with the possibility of positional disorder across a mirror plane, it is also consistent with the general observation that maximum thermal displacement occurs normal to chemical bonds and directions of steric interference. The F1, F2 and F3 thermal ellipsoids may hence be elongated normal both to their Zr—F bonds and to the non-bonding interactions between nearest-neighbor F atoms in the pentagonal ring, for which $\langle d_{F-F} \rangle = 2.5\,(1)$ Å is significantly less than $2r_{ionic}$, *i.e.* 2×1.36 Å (Pauling, 1960). Ellipsoidal elongations are thus expected normal to the mirror plane. It is noteworthy that the thermal ellipsoid of F4, the only non-H atom unconstrained either by symmetry or by close interaction, is relatively spherical with $\Delta_{max}/\Delta_{min} = 1.14$, whereas $\Delta_{max}/\Delta_{min} = 1.44$–2.3 for all other non-H atoms, where Δ is the principal r.m.s. atomic displacement.

Participation in this work by M. R. Bauer, a senior undergraduate student at Southern Oregon University, formed part of the requirements for the BS degree. Support of this research by the National Science Foundation (DMR-9708246, DMR-0137323) and, in part, by Cancer Center Support CORE Grant P30 CA 21765 is gratefully acknowledged, as is that of the American Lebanese Syrian Associated Charities (ALSAC) by C. R. Ross. It is also a pleasure to thank the referees for their perceptive comments.

References

Abrahams, S. C. (1997). *Acta Cryst.* A**53**, 673–675.
Abrahams, S. C. & Keve, E. T. (1971). *Acta Cryst.* A**27**, 157–165.
Abrahams, S. C., Mirsky, K. & Nielson, R. M. (1996). *Acta Cryst.* B**52**, 806–809.
Akella, A. & Keszler, D. A. (1994). *Acta Cryst.* C**50**, 1974–1976.
Allen, F. H. & Kennard, O. (1993). *Chem. Des. Autom. News*, **8**, 1; 66–69.
Bauer, M. R., Pugmire, D. L., Paulsen, B. L., Christie, R. J., Arbogast, D. J., Gallagher, C. S., Raveanne, W. V., Nielson, R. M., Ross, C. R. II, Photinos, P. & Abrahams, S. C. (2001). *J. Appl. Cryst.* **34**, 47–54.
Bauer, M. R., Ross, C. R. II, Nielson, R. M. & Abrahams, S. C. (1999). *Inorg. Chem.* **38**, 1028–1030.
Bergerhoff, G., Hundt, R., Sievers, R. & Brown, I. D. (1983). *J. Chem. Inf. Comput. Sci.* **23**, 66–69.
Brown, I. D. & Altermatt, D. (1985). *Acta Cryst.* B**41**, 244–247.
Bukvetskii, B. V., Gerasimenko, A. V. & Davidovich, R. L. (1990). *Koord. Khim.* **16**, 1479–1484.
Bukvetskii, B. V., Gerasimenko, A. V. & Davidovich, R. L. (1992). *Koord. Khim.* **18**, 576–579.
Casas, J. S., Castiñeiras, A., Couce, M. D., Sordo, J. & Varela, J. M. (1994). *Acta Cryst.* C**50**, 1265–1267.
Davidovich, R. L., Medkov, M. A., Rizaeva, M. D. & Bukvetskii, B. V. (1982). *Izv. Akad. Nauk SSSR Ser. Khim.* pp. 1447–1452.
Enraf–Nonius (1989). *CAD4 Diffractometer Reference Manual.* Enraf–Nonius, Delft, The Netherlands.
Hamilton, W. C. & Abrahams, S. C. (1970). *Acta Cryst.* A**26**, 18–24.
Johnson, C. K. (1976). *ORTEP*II. Report ORNL-5138, Oak Ridge National Laboratory, Tennessee, USA.
Mackay, S., Dong, W., Edwards, C., Henderson, A., Gilmore, C., Stewart, N., Shankland, K. & Donald, A. (1999). *MaXus Users Manual.* University of Glasgow, Scotland.
Nolan, B. (1967). *Acta Chem. Scand.* **21**, 2457–2462.

Papiernik, R., Mercurio, D. & Frit, B. (1982). *Acta Cryst.* B**38**, 2347–2353.
Pauling, L. (1960). *The Nature of the Chemical Bond*, 3rd ed. Ithaca: Cornell University Press.
Rodriguez, A. M., Martinez, J. A., Caracoche, M. C., Rivas, P. C., Lopez Garcia, A. R. & Spinelli, S. (1985). *J. Chem. Phys.* **82**, 1271–1274.
Ross, C. R. II, Bauer, M. R., Nielson, R. M. & Abrahams, S. C. (1999). *Acta Cryst.* B**55**, 246–254.
Ross, C. R. II, Paulsen, B. L., Nielson, R. M. & Abrahams, S. C. (1998). *Acta Cryst.* B**54**, 417–423.
Shannon, R. D. (1976). *Acta Cryst.* A**32**, 751–767.
Sheldrick, G. M. (1997). *SHELXL*97. University of Göttingen, Germany.